The Impact of Improved Aerosol Priors on Near-Infrared Measurements of Carbon Dioxide

Robert R. Nelson[1] and Christopher W. O'Dell[2]

[1]Colorado State University, Fort Collins, CO, USA
[2]Cooperative Institute for Research in the Atmosphere, Fort Collins, Colorado, USA

Correspondence: Robert R. Nelson (rrnelson@colostate.edu)

Abstract.

The Orbiting Carbon Observatory-2 (OCO-2) was launched in 2014 with the goal of measuring the column-averaged dry-air mole fraction of carbon dioxide (X_{CO_2}) with sufficient precision and accuracy to infer regional carbon sources and sinks. One of the primary sources of error in near-infrared measurements of X_{CO_2} is the scattering effects of cloud and aerosol layers.

5 In this work, we study the impact of ingesting intelligent aerosol priors from the Goddard Earth Observing System Model, Version 5 (GEOS-5) into the OCO-2 ACOS V8 retrieval algorithm with the objective of reducing the error in X_{CO_2} from real measurements. Multiple levels of both aerosol setup complexity and uncertainty on the aerosol priors were tested, ranging from a mostly unconstrained aerosol optical depth (AOD) setup to ingesting full aerosol profiles with high confidence. We find that using co-located GEOS-5 aerosol types and AODs with low uncertainty results in a small improvement in the retrieved

10 X_{CO_2} against the Total Carbon Column Observing Network relative to V8. In contrast, attempting to use modeled vertical information in the aerosol prior to improve the X_{CO_2} retrieval generally gives poor results, as aerosol models struggle with the vertical placement of aerosol layers. To assess regional differences in X_{CO_2}, we compare our results to a global CO_2 model validation suite. We find that the GEOS-5 setup performs better than V8 over Northern Africa and Central Asia, with the standard deviation of the X_{CO_2} error reduced from 2.12 ppm to 1.83 ppm, due to a combination of smaller prior AODs and

15 lower prior uncertainty. In general, the use of more intelligent aerosol priors shows promise but is currently restricted by the accuracy of aerosol models.

1 Introduction

Earth's climate is changing and anthropogenic emissions of greenhouse gases (GHGs) are the primary cause (Stocker et al., 2014). In order to quantify how the climate is changing and what might happen in the future, society needs a reliable method

20 of measuring GHGs. These measurements can then be fed into models to make them more accurate. In 1958, the first regular atmospheric measurements of the most important GHG, carbon dioxide (CO_2), were established by Charles David Keeling at the South Pole and in Hawaii on Mauna Loa. Since then, levels of CO_2 have been observed by additional ground measurement stations and, more recently, satellites orbiting the earth. These CO_2 measurements are then used in carbon flux inversion models to infer regional sources and sinks. Only about half of the carbon dioxide emitted from the burning of fossil fuels

actually remains in the atmosphere. The other half is absorbed by so-called sinks on Earth's surface. Both the land and ocean are capable of absorbing CO_2 but the partitioning between the two surfaces is uncertain, as well as how different land surface types absorb CO_2 (Le Quéré et al., 2009). For example, a sandy desert likely absorbs less atmospheric CO_2 than a cornfield in the growing season. Space-based measurements of CO_2 are one of the best methods available to investigate GHGs, their

5   sources and sinks, and how they impact Earth's climate now and in the future. This is because space-based measurements provide vastly more global coverage than the current network of ground-based measurements and, when ingested into carbon flux inversion models, could help answer these questions (Rayner and O'Brien, 2001; Baker et al., 2010; Chevallier et al., 2007, 2009). However, the precision requirements needed to gain information about the carbon cycle compared to only having ground-based measurements is about 1-2 parts-per-million (ppm) (Miller et al., 2007; Chevallier et al., 2007; Baker et al.,

10 2010). Even a bias of a few tenths of a ppm may be detrimental to carbon flux inversion models (Basu et al., 2013; Chevallier et al., 2014). Because of this, it is important to reduce errors and biases in space-based measurements of CO_2.

Currently, there are a small but growing number of satellites in orbit around Earth designed to measure the column-averaged dry-air mole fraction of CO_2, or X_{CO_2}, using reflected, near-infrared sunlight. They are the Greenhouse Gases Observing Satellite (GOSAT; Yokota et al., 2009), the Orbiting Carbon Observatory-2 (OCO-2; Crisp et al., 2008), and TanSat (Yang

15 et al., 2018). Thermal infrared instruments, such as the Atmospheric Infrared Sounder (Susskind et al., 2003) and the Infrared Atmospheric Sounding Interferometer (Pougatchev et al., 2009), can measure CO_2 in certain parts of the atmosphere, but are typically not sensitive near the surface, where the fluctuations in CO_2 are greatest. Thus, near-infrared measurements of X_{CO_2} currently provide the most valuable information on CO_2 in the atmosphere. This work is focused on the X_{CO_2} retrieval algorithm applied to measurements from OCO-2. OCO-2 is in a sun-synchronous orbit in the NASA Afternoon-Train (L'Ecuyer

20 and Jiang, 2010) and has eight adjacent footprints that each measure approximately 1.25 km by 2 km. It takes approximately 1,000,000 measurements a day, of which on average 100,000 are cloud-free.

One of the main sources of error in space-based measurements of X_{CO_2} is the scattering of sunlight by clouds and aerosols. This is because these contaminants can modify the light path seen by the satellite's sensor in ways that are difficult to quantify. Completely neglecting clouds and aerosols in measurements of X_{CO_2} can result in errors that exceed 1% (around 4 ppm of

25 CO_2) and can be much larger for scenes containing significant contamination (O'Brien and Rayner, 2002; Aben et al., 2007; Butz et al., 2009). Even when scenes are heavily screened to remove clouds and aerosols, a non-scattering retrieval performs 20-40% worse than one that includes some way to account for scattering effects (Nelson et al., 2016).

Typically, one or more pieces of information about clouds and aerosols are solved for in addition to X_{CO_2}. Some common methods include retrieving various optical properties of an aerosol type (Kuang et al., 2002; Yokota et al., 2009; Butz et al.,

30 2011), retrieving vertical aerosol information (Crisp et al., 2010; Parker et al., 2011; Butz et al., 2011; Reuter et al., 2016), retrieving parameters directly related to the photon path length (Oshchepkov et al., 2008), and parameterizing aerosols with a single isotropic scattering layer (Reuter et al., 2017). All these methods are intended to act as proxies to the real scattering effects of clouds and aerosols in the column in order to allow an accurate X_{CO_2} to be retrieved. However, it is not clear that any one method is best. The current operational OCO-2 X_{CO_2} retrieval algorithm, known as Atmospheric Carbon Observations

35 from Space (ACOS; O'Dell et al., 2012; Crisp et al., 2010) version 8 (V8; O'Dell et al., 2018), includes nine parameters related

to clouds and aerosols, which describe an ice cloud, water cloud, and three aerosol types. However, retrieved aerosol optical depths (AODs) from ACOS generally compare poorly to the highly accurate AErosol RObotic NETwork (AERONET, Holben et al., 1998; Nelson et al., 2016). This indicates that the way ACOS handles the scattering effects of clouds and aerosols can potentially be improved.

5   One choice that impacts how well the retrieved cloud and aerosol parameters perform is the use of prior information to constrain the problem. Often, a constant or climatological value with high uncertainty applied to it is used for the aerosol setup. In this work, we test the hypothesis that using more realistic aerosol priors will allow the retrieved aerosol parameters to better represent the scattering of light in the column and thus reduce the error in retrieved X_{CO_2}. Specifically, we examine the impact of using co-located modeled aerosols from the Goddard Earth Observing System Model, Version 5 (GEOS-5) as

10   prior information on the retrieved X_{CO_2} from real OCO-2 measurements. Global atmospheric models, such as GEOS-5, are highly sophisticated and contain many layers of complex physics to represent aerosol processes in the atmosphere including aerosol dynamic schemes and size-resolved aerosol microphysics (Mann et al., 2014). However, atmospheric models do not perfectly represent reality. There are still large differences between individual models, which are restricted by uncertainties in aerosol emission source characteristics, knowledge of atmospheric processes, and the meteorological field data used (Dubovik

15   et al., 2008). Despite this, it is hypothesized that these models will still be of use in the X_{CO_2} retrievals. We also examine the uncertainties applied to the aerosol priors in the current OCO-2 X_{CO_2} retrieval algorithm to see if using a lower uncertainty, in conjunction with a more realistic aerosol prior, results in an improvement in X_{CO_2} against multiple validation sources. Finally, we test whether vertical aerosol information from GEOS-5 can be successfully ingested. These results impact not only OCO-2, but X_{CO_2} from GOSAT, TanSat, and several other future space-based GHG missions that will also be significantly influenced

20   by the scattering effects of clouds and aerosols.

Section 2 gives an overview of the OCO-2 ACOS X_{CO_2} retrieval algorithm and the prior information it uses. Section 3 discusses the two validation datasets used in this study along with filtering and bias correction. Section 4 describes our use of instantaneous modeled aerosols as prior information in the retrieval while Sec. 5 presents the results. Section 6 summarizes the study's results and determines if the use of more realistic modeled aerosols is beneficial in near-infrared retrievals of X_{CO_2}.

25 2 X_{CO_2} Retrieval Algorithm

In this section, we will discuss the current OCO-2 retrieval algorithm, ACOS V8, and its cloud and aerosol parameterization. The remote sensing of CO_2 using reflected near-infrared sunlight is typically accomplished by measuring absorption in an oxygen line and one or more CO_2 lines. For OCO-2, GOSAT, and TanSat, the O_2 A-band at 0.76 μm is used in conjunction with a weak CO_2 absorption band at 1.6 μm and a strong CO_2 absorption band at approximately 2.0 μm. The main purposes

30   of the O_2 band are to estimate the path length of the photons detected by the satellite and to filter out clouds and aerosols (by screening for large variations from the expected path length). As there are only 1.5-2.0 pieces of information about the vertical

distribution of CO_2 from OCO-2 (Connor et al., 2008), the column-averaged dry-air mole fraction of carbon dioxide (X_{CO_2}) is reported:

$$X_{CO_2} = \frac{\int_0^\infty N_{CO_2}(z)dz}{\int_0^\infty N_d(z)dz} \tag{1}$$

where $N_{CO_2}(z)$ is the molecular number density of carbon dioxide and $N_d(z)$ is the molecular dry air number density at altitude z. An optimal estimation technique (Rodgers, 2000) is used to retrieve carbon dioxide and several other parameters that the measured radiances are sensitive to. Generally, optimal estimation takes a state vector containing priors with associated uncertanties, solves a cost function iteratively to find its minimum value, and outputs an optimized state vector with posterior uncertainties for each variable. A full description of the state vector and retrieval technique of the latest OCO-2 algorithm (V8) can be found in O'Dell et al., 2018. The state vector contains approximately 60 elements, including 20 vertical levels of CO_2, surface pressure, band-dependent surface albedo, total column water vapor, a temperature profile offset, several cloud and aerosol parameters, and others. The aerosol setup contains five particle types: a water cloud, ice cloud, two aerosol types from a Modern-Era Retrospective analysis for Research and Applications, Version 2 (MERRA-2; Rienecker et al., 2011) climatology, and a stratospheric aerosol type. This MERRA-2 climatology is simply the monthly means for one year for each of the five MERRA-2 aerosol types (dust, organic carbon, black carbon, sea salt, sulfate). The two types chosen to be included in the state vector are the two with the highest climatological mean AOD for a given month and location. For example, if dust and organic carbon are the two largest AODs of the possible five in the month of July for a given location, then they are selected as the two types to be retrieved for any July OCO-2 sounding for that location. The vertical profile of these aerosol types are described by Gaussians. The height and magnitude of the Gaussian are retrieved for each of the two aerosol types, water cloud, and ice cloud. The magnitude of the stratospheric aerosol type is solved for, but the height is fixed. The widths of the five Gaussian profiles are fixed, as it has been shown that the radiances are not especially sensitive to the width of a cloud or aerosol layer (Butz et al., 2009; Frankenberg et al., 2012). The prior Gaussian profiles are shown in Fig. 1, from O'Dell et al., 2018.

Thus, nine parameters are included in the state vector that directly describe the clouds and aerosols in the scene. Additionally, the natural log of the AOD is the parameter solved for that describes the magnitude of each Gaussian. This is to prevent the algorithm from attempting to retrieve a negative AOD. The retrieved height of the Gaussian represents the fraction of the surface pressure. For example, if the surface pressure is 1000 hPa and the retrieved height parameter is 0.5, the Gaussian profile will be centered at 500 hPa.

3 Data

In this work, we use two datasets to evaluate the quality of the OCO-2 X_{CO_2} retrievals in the context of testing the aerosol parameterization. While we expect the retrieved aerosol parameters to improve with the use of a more accurate prior, the retrieved aerosols are still only designed to be effective scattering parameters and thus we will not evaluate their quality in this work. The first validation dataset is 32,175 retrievals co-located with 13 Total Carbon Column Observing Network (TCCON;

Wunch et al., 2011) and AERONET sites across the globe. The second is a 30,827 retrievals matched with an ensemble of global CO_2 models where we consider the truth the median of the CO_2 models in places where they agree to within 1 ppm. These two validation sets complement each other in that TCCON is known to be highly accurate, but with limited spatial coverage. The model validation dataset likely has larger uncertainty than TCCON, but provides excellent spatial coverage.

3.1 TCCON/AERONET Validation Dataset

The TCCON validation dataset contained 32,175 OCO-2 measurements taken from 17 September 2014 to 2 May 2016. We co-located the OCO-2 measurements in time and space with the AERONET and TCCON, which were required to both be present and operational at a given site. The co-location criteria was within 1 degree latitude/longitude and +/- 30 minutes and the sites selected for use are shown in Fig. 2. As TCCON stations are all located on land, only a small fraction of co-located soundings are over water surfaces.

Table 1 lists the TCCON sites used in this study. The soundings were selected from a set of OCO-2 "lite" files (Osterman et al., 2017) that had been pre-filtered (see Sec. 3.3). We then post-processed the retrievals with multiple custom filters in an attempt to remove all scenes contaminated by clouds or aerosols.

3.2 Model Validation Dataset

Besides validation against the highly accurate but sparsely located TCCON, a set of global CO_2 models was assembled in order to examine spatial errors. We co-located 30,827 OCO-2 soundings in time and space with a suit of nine global carbon models (Peters et al., 2007; Feng et al., 2011; Baker et al., 2010; Liu et al., 2017; Crowell et al., 2018; Rödenbeck, 2005; Inness et al., 2013; Basu et al., 2013). Only points where all the models agreed to within 1 ppm of X_{CO_2} were used. Work by O'Dell et al., 2018 has shown that using this methodology produces similar error statistics to that of the TCCON validation. The median X_{CO_2} of the nine models for each of the 30,827 soundings was used as the truth metric. The OCO-2 soundings were selected by sorting all the measurements into a 4x4 degree spatial grid and filling all grid boxes with up to 10 soundings. This allowed for excellent global coverage while limiting the demand on the available computational resources needed to run the retrievals.

3.3 Filtering and Bias Correction

As OCO-2 struggles with scenes containing clouds and aerosols, multiple strategies are used to try and filter out any scene that is contaminated by scattering particles. For both validation datasets, the O_2 A-band Preprocessor (ABP; Taylor et al., 2016) and Iterative Maximum A-Posteriori Differential Optical Absorption Spectroscopy (IMAP-DOAS) Preprocessor (IDP; Frankenberg et al., 2005) were applied to every measurement before being selected to run through the retrieval. For each validation set, the approximately 30,000 soundings used in this study were those that had successfully passed through the preprocessors. These soundings were determined to be clear enough to be run through the retrieval. After removing soundings that failed to converge, post-processing filtering techniques were applied to remove additional low-quality retrievals that were not screened out by the preprocessors. These filters included the reduced χ^2, a delta pressure parameter (from ABP), and the

CO_2 and H_2O ratios (from IDP). Thus, all tests are being done on a mostly clear-sky dataset and conclusions cannot be drawn about how these retrieval modifications impact the results if scenes with thick cloud or aerosol layers are present. Additionally, as the TCCON stations are located on land, the final post-filtered validation dataset only contained land measurements and thus no conclusions can be made about OCO-2 measurements over ocean for the TCCON validation study.

5   Despite heavy pre- and post-filtering of the dataset to remove cloud and aerosol layers, no atmospheric column is truly free from scattering particles. Thus, a bias correction is typically applied to the final X_{CO_2} in an attempt to mitigate retrieval errors (O'Dell et al., 2018). In the operational V8 product, considerable effort is put into developing a multi-parameter bias correction that reduces the X_{CO_2} bias against several independent truth metrics. In this work, a single parameter bias correction was selected for each validation dataset for simplicity and to ensure a fair comparison across different setups. Additionally, it is
10 hypothesized that an improved aerosol setup might reduce the need for a complex bias correction. The parameter chosen was that which had the largest correlation with X_{CO_2} error. When comparing to TCCON, the retrieved X_{CO_2} was bias corrected by removing a linear fit between the X_{CO_2} error (retrieved X_{CO_2} - TCCON X_{CO_2}) and the difference between the retrieved surface pressure and the prior surface pressure ("dp"). This was the most correlated parameter in the majority of our TCCON tests and thus was selected as the bias correction parameter. This parameter is correlated with X_{CO_2} biases because any
15 unparameterized clouds and aerosols in the column can make the retrieval think there is a lower surface pressure than in reality. Thus, bias correcting this mistake out is designed to bring the retrieved surface pressures back to realistic values and can approximately account for the improperly parameterized clouds and aerosols. In the case of the model validation dataset, the bias correction parameter was the solar zenith angle. Physically, this represents the removal of artificial biases induced by longer air masses. The reason why this parameter was selected over dp is that the model dataset has excellent latitudinal coverage and
20 thus the air mass is weighted more than dp. TCCON, however, is spatially limited and thus the air mass dependence is not as prevalent when searching for optimal bias correction parameters.

4   Modeled Aerosol Priors

As discussed in section 2, the OCO-2 retrieval algorithm has several aerosol parameters in its state vector. The prior values for most of these parameters in V8 are fixed or taken from a monthly climatology. Here, we discuss several methods in which we
25 test the use of instantaneous, 3D modeled aerosol data as prior information to improve upon the current priors with the hope of increasing the precision and accuracy of the final OCO-2 X_{CO_2} product.

The GEOS-5 Forward Processing for Instrument Teams (GEOS-5 FP-IT; Rienecker et al., 2008) weather forecasting model, created and maintained by the NASA Global Modeling and Assimilation Office, is designed specifically for instrument teams in that the entire period (2000-current) is run using the same GEOS-5 version to maintain consistency and avoid any unwanted
30 biases from updates to the model. For this work, GEOS-5 FP-IT version 5.12.4, hereafter referred to as GEOS-5, was co-located in time and space with the OCO-2 soundings. GEOS-5 is on a 0.625-degree longitude by 0.5-degree latitude horizontal grid with 72 vertical layers extending to 0.01 hPa with a time-step of 3 hours. The model was linearly interpolated in space and the nearest 3-hour model update was chosen in time. For example, if the OCO-2 sounding was taken at 1900 UTC, the 1800 UTC

model run was used. The GEOS-5 aerosol scheme contains 15 different types with up to five different size bins for each type, which we aggregate into five unique types: dust, organic carbon, black carbon, sea salt, sulfate. The aggregation process weights by the typical relative amount of optical depth contributed by each type at 760 nm and uses a typical relative humidity value for the hygroscopic types. Each type has a unique optical properties, including the single scatter albedo, extinction coefficient,

5   and refractive index. Further details can be found in Crisp et al., 2010. GEOS-5 ingests Terra Moderate Resolution Imaging Spectroradiometer (MODIS; Kaufman et al., 1997) AOD, Aqua MODIS AOD, and Multi-angle Imaging SpectroRadiometer (MISR; Martonchik et al., 1998) aerosol information. AERONET measurements are not used for this product as the data latency is unacceptably large. Figure 3 shows that GEOS-5 AODs correlate better with AERONET compared to both the climatological MERRA-2 AODs and the corresponding retrieved AOD values from OCO-2 V8. Thus, using the model and assigning it some

10 confidence should result in an improved correlation in retrieved OCO-2 AODs compared to AERONET.

Our primary hypothesis in this work is that using instantaneous modeled aerosol data as prior information will result in smaller X_{CO_2} errors when compared to the current operational setup that uses a monthly climatology. Figure 4 shows the first of the two aerosol types selected when using the MERRA-2 monthly climatology and when using the interpolated GEOS-5 model field. Certain features, such as Saharan dust and biomass burning, are generally realistically placed in the climatology

15 but the day-to-day variations of the atmosphere are not present and thus the climatology is not representative of the true state of the atmosphere for a given OCO-2 sounding location. For example, dust is selected over large portions of the high northern latitudes in the GEOS-5 model field, but rarely in the MERRA-2 monthly climatology.

Three methods of varying complexity were chosen to ingest the instantaneous model data:

– Using the top two aerosol types and their corresponding AODs

20 – Using the top two aerosol types and fitting a Gaussian to the vertical profile of both types

– Using the top two aerosol types and solving for a scale factor on an interpolated 20-layer aerosol profile

The methodology for selecting which two (of the five) aerosol types to be included in the state vector is simply sorting them by AOD at 760 nm and selecting the two largest values. The ice cloud, water cloud, and stratospheric aerosol type were always retrieved. The ice cloud and water cloud characteristics were kept the same as V8, while the stratospheric aerosol's optical

25 depth prior and corresponding uncertainty were determined by our setups described below.

4.1   Types and Optical Depths

The first method simply takes the top two aerosol types based on sorting by each type's AOD and uses their corresponding AODs as prior information for each type. This method is the simplest of our tests and does not rely on any modeled vertical aerosol information.

4.2 Types and Gaussian Fits

The second method takes the largest two aerosol types, as before. The 72-layer GEOS-5 aerosol profiles for both types are then interpolated onto the 20-layer OCO-2 vertical grid. A Gaussian is then fit to that 20-layer profile and the magnitude (optical depth, τ), height, and width of that Gaussian are fed in to the retrieval as prior information. An example is shown in Fig. 5.

5   Occasionally, the fit is a poor representation of the vertical profile. This is often the case with the sulfate type, which can have both a lower tropospheric peak and a stratospheric peak, resulting in a profile that cannot be represented with a single Gaussian. To avoid this issue, the sulfate type, if selected, was fit to below 400 hPa and the stratospheric aerosol type (discussed in Sec. 2) was a separate Gaussian fit for the profile above 400 hPa. This method was chosen to test the hypothesis that ingesting vertical information from the model will lead to an improved parameterization of the scattering and, subsequently, a more accurate

10   X_{CO_2}.

4.3 Types and Scale Factors

The third and most complex method takes the largest two aerosol types sorted by AOD, as before. The 72-layer GEOS-5 aerosol profiles for both types are then interpolated onto the 20-layer OCO-2 vertical grid. A scale factor applied to the interpolated profile is then solved for by the retrieval. Because the ACOS retrieval solves for the natural log of the AOD, we solve for an

15   additive scalar which acts as a multiplicative scaling factor when converted to AOD. This means that if the retrieval determines that the scale factor should be 1.5, the GEOS-5 AOD profile magnitude will be multiplied by 1.5. This method is similar to that of Parker et al., 2011, except here we are using a vertical aerosol profile co-located in time and space as the prior, while they use a constant aerosol profile. This method was chosen to test the hypothesis that Gaussian fits are insufficient to realistically parameterize the shapes of true vertical aerosol profiles in the X_{CO_2} retrieval.

20   ## 4.4 Aerosol Prior Uncertainties

In addition to these three techniques used to modify the aerosol priors, the prior uncertainty must also be considered when using optimal estimation. In the operational ACOS X_{CO_2} retrieval algorithm, the uncertainty on the aerosol parameters is typically very loose. For example, a prior AOD of 0.1 is approximately -2.3 in ln-space. Assigning the V8 uncertainty of 2.0 to $\ln(\tau)$ gives 1-sigma values of -4.3 and -0.3 in ln-space, which equates to about 0.014 and 0.74 in optical depth. This large prior uncertainty

25   is due to the lack of confidence in the monthly climatological priors and because it is believed that the radiances themselves should provide enough information to properly constrain the results. However, using this new instantaneous setup allows us to decrease the prior uncertainty because we have more confidence in the GEOS-5 model compared to the monthly climatology, as demonstrated by Fig. 3. The three setups chosen to test are using the operational uncertainty ("high uncertainty"), 25% of the operational uncertainty ("low uncertainty"), and fixing the prior aerosol values ("no uncertainty"). For example, using our

30   first method above (Sec. 4.1) with low uncertainty means solving for the AODs of the two selected aerosol types with 25% of the operational uncertainty assigned to the prior values. This means that instead of a 1-sigma uncertainty of 2.0 on $\ln(\tau)$, we assign a value of 0.5. This equates to a 1-sigma uncertainty range of between 0.06 and 0.16 on a prior AOD of 0.1. Table 2

lists all the test setups and the corresponding uncertainties on the retrieved $\ln(\tau)$ and, except for the scalar profile tests, the retrieved height. The third method, solving for a 20-layer profile (Sec. 4.3), does not lend itself to assigning single values of uncertainty equivalent to the other two setups. Thus, we assigned layer uncertainties of $\ln(10)$, 0.5, and 0.001 for each layer to represent the operational, low, and fixed setups. We also ran the operational retrieval with low and no uncertainty on the AODs

5 in an attempt to isolate the impact of only modifying the prior uncertainties. When ingesting vertical information in the second and third methods, we also reduced the uncertainty of the retrieved height. The width was effectively never retrieved, as it was always assigned an uncertainty of 0.001.

After processing all 12 retrieval variants, applying similar post-filtering, and matching soundings to ensure a fair comparison, 19,471 soundings remained in the TCCON validation dataset while 17,355 soundings remained in the model validation dataset.

10 For both datasets and all tests, there were no significant outliers when it came to the percentage of soundings that converged or remained after post-filtering. Typically, the retrievals with loose priors had slightly more soundings fail to converge and the more complex retrieval schemes lost more soundings in post-filtering, but only by a few hundred soundings.

5   Results

In this section we discuss the impact of using more intelligent aerosol priors in the OCO-2 X_{CO_2} retrieval by comparing our

15 test setups to both TCCON and an ensemble of global X_{CO_2} models.

5.1   TCCON Validation Results

Figure 6 shows the results of our test setups alongside the operational retrieval variants (top row). Here, we can see the impact that different prior information and different prior uncertainties have on the retrieved X_{CO_2} when compared to TCCON.

For our nine GEOS-5 test setups, when examining the standard deviation of the error (σ), correlation coefficient (R), and

20 mean absolute error (MAE) versus TCCON, the values are typically best for the setups where only the types and the AODs are ingested (second row). When we apply a Gaussian fit to the modeled profiles and use those heights and widths as priors (third row), we see an increase in the scatter against our validation source along with a worse MAE and R. Finally, when we solve for a scalar on the modeled aerosol profile (bottom row), we see the largest scatter in X_{CO_2} against TCCON, worst correlations, and highest MAEs. It therefore appears that trying to incorporate vertical information from the aerosol model leads to a worse

25 X_{CO_2}.

The only GEOS-5 test setup with errors and a correlation coefficient better than the operational retrieval is the middle panel of the second row (green triangles), where the types and AODs were ingested with low uncertainty. This may indicate that it is reasonable to assign some confidence in the modeled AODs from GEOS-5, rather than leaving it mostly unconstrained. The operational retrieval with low uncertainty (blue triangles) does relatively well, but slightly worse than the original V8 (blue

30 squares).

For all retrieval setups, fixing the aerosol input (right column) results in worse error statistics. This is likely because models are not perfect and by entirely removing the retrieval's ability to fit for aerosol effects on the radiances it results in large errors

in X_{CO_2}. Keeping the prior aerosol uncertainty the same as the operational retrieval (left column), however, appears to allow too much freedom and the aerosol parameters revert to the operational values, regardless of what the prior values are. This is because we are assigning almost no confidence to the prior, so all the information comes from the retrieval. This shows the utility of having semi-constrained aerosol priors to guide the X_{CO_2} retrieval algorithm. The only row where the low uncertainty

5 test does better than the high uncertainty test is when we ingest types and AODs. This again indicates that it may be beneficial to use GEOS-5 modeled types and AODs and assign them some level of confidence that is greater than the V8 constraint.

5.2 Model Validation Results

While TCCON gives a robust estimate of the statistical errors for our test setups, it does not allow for regional analysis because of the sparsity of the network. The CO_2 model median validation technique, described in Sec. 3.2, allows for an assessment of

10 regional errors in the test setups compared to a truth metric. For this work, the most promising aerosol setup in the TCCON validation study was selected for further analysis. That is, ingesting the GEOS-5 types and AODs with low uncertainty. Figure 7 shows the operational (V8) X_{CO_2} error and the GEOS-5 aerosol prior setup X_{CO_2} error while the top panel of Fig. 8 shows the difference of the absolute value of the X_{CO_2} errors for the two setups.

Here, regional differences can be seen. Over Northern Africa and Central Asia the operational retrieval (top panel of Fig. 7)

15 is often biased high, which results in a large X_{CO_2} scatter in those regions. The GEOS-5 aerosol setup (bottom panel of Fig. 7), however, shows that those high biased bins have mostly been removed. The difference plot (top panel of Fig. 8) demonstrates an improvement in the error of around 1 ppm for many grid cells in Northern Africa and Central Asia. An additional regional difference is in the Southern Ocean, where the GEOS-5 aerosol setup develops a new high bias of 0.4 ppm in many of the bins, compared to V8 which has a bias of nearly zero (+0.1 ppm). Over the remaining land and ocean regions there is minimal

20 change in X_{CO_2} between the two datasets. While of interest, comparing retrieval setups over the Amazon and high latitudes is difficult due to the lack of soundings. This is because these regions are typically cloudy around solar noon or lack the necessary amount of reflected sunlight to make an accurate retrieval, respectively, so they have been filtered out.

Regarding the plots just discussed, three factors could be contributing to the regional changes in X_{CO_2} between V8 and the GEOS-5 aerosol prior setup. First, the decrease in uncertainty to 25% of V8. Second, the two selected aerosol types. Third, the

25 modified AOD priors of the two aerosol types. In order to isolate the first effect, the middle panel of Fig. 8 shows a comparison between V8 and V8 with low uncertainty. Here, we can see that the impact of simply reducing the prior uncertainty on the retrieved AODs is substantial and accounts for a considerable portion of the improvement over Northern Africa and Central Asia, with the standard deviation of the error being reduced from 2.12 ppm to 1.92 ppm. The ocean remains nearly unchanged, along with much of the remaining land surface.

30 Now that we have isolated the impact of reducing uncertainty, we can compare V8 with low uncertainty to GEOS-5 types & AODs with low uncertainty to determine what impact, if any, using the constrained GEOS-5 aerosol types and priors has on the X_{CO_2} error. The bottom panel of Fig. 8 shows that this change is beneficial over Central Asia ($\sigma_{X_{CO_2}\ error}$ reduced from 2.07 ppm to 1.94 ppm for measurements over land between latitudes 16 N and 56 N and longitudes 52 E and 152 E), has a minimal effect over the Northern Africa ($\sigma_{X_{CO_2}\ error}$ changed from 1.63 ppm to 1.62 ppm for measurements over land

between latitudes 6 S and 38 N and longitudes 20 W and 52 E), and a detrimental effect over the Southern Ocean ($\sigma_{X_{CO_2}\ error}$ increased from 1.86 ppm to 1.95 ppm and a positive bias of 0.4 ppm for measurements south of 45 S). This suggests that the improvement in the scatter of the X_{CO_2} error against model validation over the Northern Africa was primarily due to the reduction in uncertainty in the prior AODs, and not the co-located GEOS-5 aerosol prior types and values themselves. Over

5 Central Asia, however, the improvement seems to be a combination of reducing the uncertainty and using instantaneous types and/or AODs. Over the Southern Ocean, using GEOS-5 types and prior AODs results in an increase in scatter and a high bias of 0.4 ppm.

Next, we attempt to distinguish between the impact of using GEOS-5 aerosol types and using their corresponding AODs as prior information. The areas of interest are Central Asia, where using instantaneous priors improved the X_{CO_2} retrieval,

10 and the Southern Ocean, where it worsened the X_{CO_2} retrieval. The top panel of Fig. 9 shows the binned prior AOD for V8, which is derived from a monthly MERRA-2 climatology (as discussed in Sec. 2), while the bottom panel shows the binned prior AOD for our test setup which uses the co-located GEOS-5 modeled data. In general, slightly more variation is seen in the GEOS-5 priors, which is to be expected, as the monthly climatology is a mean of an entire month and thus removes most synoptic variability. The most prominent change, however, is the significant reduction in prior AOD over Northern Africa and

15 Central Asia. The GEOS-5 aerosol setup has a 30% lower mean prior AOD than V8. This is likely because the MERRA-2 climatology was created by simply averaging an entire month of data together, including all instances where the optical depth was large due to dust storms, pollution events, biomass burning, etc. Those scenes, however, are typically removed by OCO-2's pre-screeners (ABP and IDP, described in Sec. 3.3) before being processed through the retrieval code and thus the GEOS-5 prior map only includes scenes that were determined to be sufficiently clear to perform retrievals on. This suggests that the

20 MERRA-2 monthly climatology aerosol prior may be artificially high and not entirely appropriate for use in the operational retrieval algorithm. This is also seen in Fig. 3, where there are several MERRA-2 climatology AODs that are significantly high biased against AERONET. Fig. 3, however, is only data from 13 AERONET sites and is thus not representative of the global differences.

In optimal estimation the final, optimized state vector represents a weighted combination of the prior information and the

25 measurement, not just the state of the prior. The top panel of Fig. 10 shows the retrieved AOD for V8 while the bottom panel shows the retrieved AOD for the GEOS-5 aerosol setup. Here, we see an even more dramatic difference in retrieved AODs over the Northern Africa and Central Asia. Over land in these two regions, the retrieved AOD is 52% lower for the GEOS-5 aerosol setup. This is partially due to the reduced uncertainty on the prior AODs for the GEOS-5 aerosol setup, which prevents it from deviating substantially from the prior.

30 While the differences in X_{CO_2} over Central Asia correlate with a large difference in the magnitude of the retrieved AOD, the same cannot be said of the X_{CO_2} differences over the Southern Ocean, as those differences in retrieved AOD are small (8.9% increase in the GEOS-5 test setup over the Southern Ocean). Additionally, the middle panel of Fig. 8 demonstrated that the reduction in uncertainty alone had a minimal impact on this region.

The changing of one or both of the aerosol types when going from the MERRA-2 monthly climatology to the instantaneous

35 GEOS-5 setup could be the explanation for the positive 0.4 ppm bias in X_{CO_2}. Of the 17,355 global soundings remaining

after post-filtering, 32% have one or both aerosol types different while only 0.7% have both aerosol types different. To test this hypothesis, we ran an additional set of soundings similar to the GEOS-5 types & AODs with low uncertainty, but not changing the types. Figure 11 demonstrates that changing the types has almost no effect on the Southern Ocean and overall has a small and sporadic effect (note the reduced scale). The mean difference between ingesting GEOS-5 AODs and types

5 and only ingesting GEOS-5 AODs for soundings where the type actually changed is about 0.01 ppm with a standard deviation of about 0.2 ppm. Only a small fraction of soundings had differences larger than 0.5 ppm (2.3% of all soundings). Thus, the selection of an appropriate AOD prior and uncertainty is much more important than the exact aerosol properties in our retrieval parameterization.

After further investigation, the modification to the stratospheric aerosol prior and its corresponding uncertainty is likely the

10 cause of the Southern Ocean 0.4 ppm high bias in the GEOS-5 aerosol setup. As detailed in O'Dell et al., 2018, ACOS V7 contained a high bias over water at high southern latitudes due to both the presence of stratospheric aerosol from the Calbuco eruption in 2015 as well as ice build up on the OCO-2 focal plane arrays. Here, we have unintentionally replicated this issue, as the stratospheric aerosol priors from GEOS-5 are near zero (as opposed to a global prior value of 0.006 used in V8). Figure 12 demonstrates that when V8 solves for a large stratospheric AOD in the Southern Ocean, GEOS-5 cannot because it starts with

15 a lower prior and is unable to sufficiently increase it. This result in a significant positive bias in X_{CO_2} (bottom of Fig. 7). When the retrieved V8 stratospheric AOD is greater than 0.012 in the Southern Ocean, the GEOS-5 aerosol setup incurs a positive bias of approximately 1.4 ppm (compared to the positive 0.4 ppm bias for all Southern Ocean retrievals). This indicates that in soundings where large stratospheric AODs are needed to fit the radiances, the lack of AOD usually appears to lead to a high bias in X_{CO_2}.

20 To further test this hypothesis, we ran a set of soundings where we reverted the stratospheric aerosol prior AOD and prior uncertainty back to V8 values (0.006 and a 1-sigma uncertainty on the ln(AOD) of 1.8). This revealed that the 0.4 ppm bias in the Southern Ocean mostly disappears, as the high bias is reduced back to approximately +0.1 ppm, in agreement with V8.

6 Discussion and Conclusions

In this study we investigated the impact of using more intelligent aerosol priors in the OCO-2 ACOS X_{CO_2} retrieval algorithm

25 applied to real measurements. We ingested aerosol information from co-located GEOS-5 model data with varying levels of uncertainty and compared to two validation sources, TCCON and a global CO_2 model suite.

We found that ingesting instantaneous AOD information with low uncertainty slightly reduced the standard deviation of the X_{CO_2} error against TCCON from 1.17 ppm to 1.13 ppm. More interestingly, we found that attempting to ingest vertical information from GEOS-5 produced poor results against TCCON, with mean absolute errors more than 50% larger than V8. We

30 hypothesize that this is because accurate vertical placement of aerosol layers still represents a significant challenge in global aerosol models (Koffi et al., 2016). This is due to the large uncertainty in processes related to how aerosols are distributed vertically, partially because of the lack of constraint by global observations (Kipling et al., 2016). Additionally, fixing the

ingested aerosol information also makes the retrieval compare poorly to TCCON. This is, again, because the priors will always be imperfect, so the OCO-2 ACOS X_{CO_2} retrieval algorithm needs some amount of freedom to adjust the radiances.

A comparison to our model validation dataset reveals an improvement over Northern Africa and Central Asia when using the GEOS-5 types and AODs with low uncertainty compared to V8, with the scatter in X_{CO_2} error being reduced from 2.12 ppm to 1.83 ppm. Additionally, we see a new high bias in X_{CO_2} of 0.4 ppm over the Southern Ocean. These regional differences in OCO-2 V8 compared to the GEOS-5 type and AOD low uncertainty prior test setup are likely caused by one of the three modifications. First, reducing the uncertainty on the prior AODs in V8 results in an improvement over Northern Africa and Central Asia. Figure 13 shows that by constraining the prior AODs in V8, we prevent the algorithm from retrieving large AODs. Those soundings that retrieved large AODs in V8 but smaller AODs in the low uncertainty setup generally have smaller X_{CO_2} errors (blue pixels in Fig. 13). For soundings where the retrieved V8 AOD is greater than 0.4 over Northern Africa and Central Asia, constraining the prior AODs with low uncertainty reduces the X_{CO_2} bias against the validation dataset by 0.55 ppm on average. Some soundings are outliers, in that they do worse when constrained (red pixels in Fig. 13). Around 8% of the retrievals have an X_{CO_2} error increase of greater than 0.5 ppm. This may be because those scenes actually contain large AODs and thus constraining the priors is hindering the retrieval's ability to properly fit the radiances, but further investigation is needed on this topic.

Second, some of the high bias seen in V8 (top panel of Fig. 7) is likely due to the MERRA-2 climatological priors being unrealistically high for the selected OCO-2 soundings. Physically, when there is too much aerosol being retrieved, the CO_2 absorption lines are filled in too much because the retrieval thinks those photons are experiencing a shorter path length than they are in reality. The retrieval then must add more CO_2 to deepen the absorption lines again to match the measured line depths. This results in the observed high bias in V8 over Central Asia, which is mostly removed when smaller, more appropriate AOD priors are taken from the GEOS-5 dataset (bottom panel of Fig. 8). However, the bottom panel of Fig. 8 also showed that using lower AOD priors alone had no significant net impact on Northern Africa. This difference may be due to Northern Africa having a higher surface albedo than Central Asia. This results in a larger fraction of the signal coming from the surface and less weight placed on any aerosols present. So long as the retrieved aerosols are not very large, as discussed above, the X_{CO_2} results over Northern Africa may be less sensitive to the aerosol prior than other regions.

Third, the GEOS-5 types & AODs with low uncertainty setup resulted in a new high bias of 0.4 ppm in X_{CO_2} relative to V8 over the Southern Ocean. It was initially hypothesized that the change in aerosol types may have caused the high bias, but we showed that changing one or both of the aerosol types has a minimal impact on the X_{CO_2} in this setup. After additional tests, we found that the GEOS-5 stratospheric AODs in the Southern Ocean were too small to be able to account for actual stratospheric aerosol in the region along with the effects of an ice accumulation artifact in the OCO-2 radiances. Reverting the stratospheric prior and uncertainty back to that of V8 mostly eliminated the high bias in the Southern Ocean. This conclusion highlights the severe impact that even a small amount of aerosols can have on the retrieved X_{CO_2}.

This work is relevant for several missions set to launch in the near future, including OCO-3, GOSAT-2, MicroCarb, Tansat-2, and GeoCarb. Algorithm development teams will have to decide how they will account for clouds and aerosols in order to minimize errors in their CO_2 measurements. While we have shown the benefits and limitations of using instantaneous modeled

aerosol data to inform the OCO-2 X_{CO_2} retrieval, more work is needed to determine the optimal aerosol parameterization for near-infrared measurements of CO_2. These results may be of use in guiding development for the next version of the OCO-2 ACOS X_{CO_2} retrieval algorithm.

5 *Acknowledgements.* The authors would like to thank Thomas E. Taylor of Colorado State University and Aronne Merrelli of the University of Wisconsin-Madison for their contributions to this work. This work was funded by NASA Jet Propulsion Laboratory OCO-2 Subcontract #5359007. TCCON data were obtained from the TCCON Data Archive, hosted by the Carbon Dioxide Information Analysis Center (CDIAC) - tccon.onrl.gov. The Caltech, Lamont, and Park Falls TCCON stations are funded by NASA grants NNX14AI60G, NNX11AG01G, NAG5-12247, NNG05-GD07G, and NASA Orbiting Carbon Observatory. The Darwin TCCON station is funded by NASA grants NAG5-12247

10 and NNG05-GD07G and the Australian Research Council grants DP140101552, DP110103118, DP0879468 and LP0562346. The Orléans TCCON station is funded by the EU projects InGOS and ICOS-INWIRE, by the Senate of Bremen and by the RAMCES team at LSCE. The Paris TCCON station is supported by UPMC.

References

Aben, I., Hasekamp, O., and Hartmann, W.: Uncertainties in the space-based measurements of CO_2 columns due to scattering in the Earth's atmosphere, Journal of Quantiterative Spectroscopy & Radiative Transfer, 104, 450–459, https://doi.org/10.1016/j.jqsrt.2006.09.013, 2007.

5 Baker, D. F., Bösch, H., Doney, S. C., O'Brien, D., and Schimel, D. S.: Carbon source/sink information provided by column CO_2 measurements from the Orbiting Carbon Observatory, Atmospheric Chemistry and Physics, 10, 4145–4165, https://doi.org/10.5194/acp-10-4145-2010, 2010.

Basu, S., Guerlet, S., Butz, A., Houweling, S., Hasekamp, O., Aben, I., Krummel, P., Steele, P., Langenfelds, R., Torn, M., Biraud, S., Stephens, B., Andrews, A., and Worthy, D.: Global CO_2 fluxes estimated from GOSAT retrievals of total column CO_2, Atmospheric
10 Chemistry and Physics, 13, 8695–8717, https://doi.org/10.5194/acp-13-8695-2013, 2013.

Butz, A., Hasekamp, O. P., Frankenberg, C., and Aben, I.: Retrievals of atmospheric CO_2 from simulated space-borne measurements of backscattered near-infrared sunlight: accounting for aerosol effects, Applied Optics, 48, 3322–3336, https://doi.org/10.1364/AO.48.003322, 2009.

Butz, A., Guerlet, S., Hasekamp, O., Schepers, D., Galli, A., Aben, I., Frankenberg, C., Hartmann, J.-M., Tran, H., Kuze, A., Keppel-Aleks,
15 G., Toon, G., Wunch, D., Wennberg, P., Deutscher, N., Griffith, D., Macatangay, R., Messerschmidt, J., Notholt, J., and Warneke, T.: Toward accurate CO_2 and CH_4 observations from GOSAT, Geophysical Research Letters, 38, https://doi.org/10.1029/2011GL047888, 2011.

Chevallier, F., Bréon, F.-M., and Rayner, P. J.: Contribution of the Orbiting Carbon Observatory to the estimation of CO_2 sources and sinks: Theoretical study in a variational data assimilation framework, Journal of Geophysical Research, 112, D09 307,
20 https://doi.org/10.1029/2006JD007375, 2007.

Chevallier, F., Maksyutov, S., Bousquet, P., Bréon, F.-M., Saito, R., Toshida, Y., and Yokota, T.: On the accuracy of the CO_2 surface fluxes to be estimated from the GOSAT observations, Geophysical Research Letters, 36, L19 807, https://doi.org/10.1029/2009GL040108, 2009.

Chevallier, F., Palmer, P. I., Feng, L., Boesch, H., O'Dell, C. W., and Bousquet, P.: Toward robust and consistent regional CO_2 flux estimates from in situ and spaceborne measurements of atmospheric CO_2, Geophysical Research Letters, 41, 1065–1070,
25 https://doi.org/10.1002/2013GL058772, 2014.

Connor, B. J., Boesch, H., Toon, G., Sen, B., Miller, C., and Crisp, D.: Orbiting Carbon Observatory: Inverse method and prospective error analysis, Journal of Geophysical Research, 113, D05 305, https://doi.org/10.1029/2006JD008336, 2008.

Crisp, D., Miller, C. E., and DeCola, P. L.: NASA Orbiting Carbon Observatory: measuring the column averaged carbon dioxide mole fraction from space, Journal of Applied Remote Sensing, 2, 023 508–023 508, https://doi.org/10.1117/1.2898457, 2008.

30 Crisp, D., Boesch, H., Brown, L., Castano, R., Christi, M., Connor, B., Frankenberg, C., McDuffie, J., Miller, C. E., Natraj, V., O'Dell, C., O'Brien, D., Polonsky, I., Oyafuso, F., Thompson, D., Toon, G., and Spurr, R.: OCO (Orbiting Carbon Observatory)-2 Level 2 Full Physics Retrieval Algorithm Theoretical Basis, Tech. Rep. OCO D-65488, Tech. rep., NASA Jet Propulsion Laboratory, California Institute of Technology, Pasadena, CA, version 1.0 Rev 4, https://docserver.gesdisc.eosdis.nasa.gov/public/project/OCO/OCO-2_L2_FP_ATBD_v1_rev4_Nov10.pdf, 2010.

35 Crowell, S. M. R., Kawa, S. R., Browell, E. V., Hammerling, D. M., Moore, B., Schaefer, K., and Doney, S. C.: On the Ability of Space-Based Passive and Active Remote Sensing Observations of CO_2 to Detect Flux Perturbations to the Carbon Cycle, Journal of Geophysical Research: Atmospheres, 123, 1460–1477, https://doi.org/10.1002/2017JD027836, 2018.

Dubey, M., Parker, H., Henderson, B., Green, D., Butterfield, Z., Keppel-Aleks, G., Allen, N., Blavier, J.-F., Roehl, C., Wunch, D., and Lindenmaier, R.: TCCON data from Manaus (BR), Release GGG2014.R0, TCCON Data Archive, hosted by CaltechDATA, https://doi.org/10.14291/tccon.ggg2014.manaus01.R0/1149274, 2014.

Dubovik, O., Lapyonok, T., Kaufman, Y. J., Chin, M., Ginoux, P., Kahn, R. A., and Sinyuk, A.: Retrieving global aerosol sources from satellites using inverse modeling, Atmospheric Chemistry and Physics, 8, 209–250, https://doi.org/10.5194/acp-8-209-2008, 2008.

Feist, D. G., Arnold, S. G., John, N., and Geibel, M. C.: TCCON data from Ascension Island (SH), Release GGG2014.R0, TCCON Data Archive, hosted by CaltechDATA, https://doi.org/10.14291/tccon.ggg2014.ascension01.R0/1149285, 2014.

Feng, L., Palmer, P. I., Yang, Y., Yantosca, R. M., Kawa, S. R., Paris, J.-D., Matsueda, H., and Machida, T.: Evaluating a 3-D transport model of atmospheric CO_2 using ground-based, aircraft, and space-borne data, Atmospheric Chemistry and Physics, 11, 2789–2803, https://doi.org/10.5194/acp-11-2789-2011, 2011.

Frankenberg, C., Platt, U., and Wagner, T.: Iterative maximum a posteriori (IMAP)-DOAS for retrieval of strongly absorbing trace gases: Model studies for CH_4 and CO_2 retrieval from near infrared spectra of SCIAMACHY onboard ENVISAT, Atmospheric Chemistry and Physics, 5, 9–22, https://doi.org/10.5194/acp-5-9-2005, 2005.

Frankenberg, C., Hasekamp, O., O'Dell, C., Sanghavi, S., Butz, A., and Worden, J.: Aerosol information content analysis of multi-angle high spectral resolution measurements and its benefit for high accuracy greenhouse gas retrievals, Atmospheric Measurement Techniques, 5, 1809–1821, https://doi.org/10.5194/amt-5-1809-2012, 2012.

Griffith, D. W. T., Deutscher, N. M., Velazco, V. A., Wennberg, P. O., Yavin, Y., Keppel-Aleks, G., Washenfelder, R., Toon, G. C., Blavier, J.-F., Paton-Walsh, C., Jones, N. B., Kettlewell, G. C., Connor, B., Macatangay, R. C., Roehl, C., Ryczek, M., Glowacki, J., Culgan, T., and Bryant, G.: TCCON data from Darwin (AU), Release GGG2014.R0, TCCON Data Archive, hosted by CaltechDATA, https://doi.org/10.14291/tccon.ggg2014.darwin01.R0/1149290, 2014.

Hase, F., Blumenstock, T., Dohe, S., Gross, J., and Kiel, M.: TCCON data from Karlsruhe (DE), Release GGG2014.R1, TCCON Data Archive, hosted by CaltechDATA, https://doi.org/10.14291/tccon.ggg2014.karlsruhe01.R1/1182416, 2015.

Holben, B. N., Eck, T. F., Slutsker, I., Tanré, D., Buis, J., Setzer, A., Vermote, E., Reagan, J. A., Kaufman, Y. J., Nakajima, T., Lavenu, F., Jankowiak, I., and Smirnov, A.: AERONET - A Federated Instrument Network and Data Archive for Aerosol Characterization, Remote Sensing of Environment, 66, 1–16, https://doi.org/10.1016/S0034-4257(98)00031-5, 1998.

Inness, A., Baier, F., Benedetti, A., Bouarar, I., Chabrillat, S., Clark, H., Clerbaux, C., Coheur, P., Engelen, R., Errera, Q., Flemming, J., George, M., Granier, C., Hadji-Lazaro, J., Huijnen, V., Hurtmans, D., Jones, L., Kaiser, J., Kapsomenakis, J., Lefever, K., Leitao, J., Razinger, M., Richter, A., Schultz, M., Simmons, A., Suttie, M., Stein, O., Thépaut, J.-N., Thouret, V., Vrekoussis, M., and Zerefos, C.: The MACC reanalysis: an 8 yr data set of atmospheric composition, Atmospheric Chemistry and Physics, 13, 4073–4109, https://doi.org/10.5194/acp-13-4073-2013, 2013.

Iraci, L. T., Podolske, J., Hillyard, P. W., Roehl, C., Wennberg, P. O., Blavier, J.-F., Allen, N., Wunch, D., Osterman, G., and Albertson, R.: TCCON data from Edwards (US), Release GGG2014.R1, TCCON Data Archive, hosted by CaltechDATA, https://doi.org/10.14291/tccon.ggg2014.edwards01.R1/1255068, 2016.

Kaufman, Y. J., Tanré, D., Remer, L. A., Vermote, E., Chu, A., and Holben, B.: Operational remote sensing of tropospheric aerosol over land from EOS moderate resolution imaging spectroradiometer, Journal of Geophysical Research: Atmospheres, 102, 17 051–17 067, https://doi.org/10.1029/96JD03988, 1997.

Kawakami, S., Ohyama, H., Arai, K., Okumura, H., Taura, C., Fukamachi, T., and Sakashita, M.: TCCON data from Saga (JP), Release GGG2014.R0, TCCON Data Archive, hosted by CaltechDATA, https://doi.org/10.14291/tccon.ggg2014.saga01.R0/1149283, 2014.

Kipling, Z., Stier, P., Johnson, C. E., Mann, G. W., Bellouin, N., Bauer, S. E., Bergman, T., Chin, M., Diehl, T., Ghan, S. J., Iversen, T., Krikevåg, A., Kokkola, H., Liu, X., Luo, G., van Noije, T., Pringle, K. J., von Salzen, K., Schulz, M., Seland, Ø., Skeie, R. B., Takemura, T., Tsigaridis, K., and Zhang, K.: What controls the vertical distribution of aerosol? Relationships between process sensitivity in HadGEM3–UKCA and inter-model variation from AeroCom Phase II, Atmospheric Chemistry and Physics, 16, 2221–2241, https://doi.org/10.5194/acp-16-2221-2016, 2016.

Kivi, R. and Heikkinen, P.: Fourier transform spectrometer measurements of column CO_2 at Sodankylä, Finland, Geoscientific Instrumentation, Methods and Data Systems, 5, 271–279, https://doi.org/10.5194/gi-5-271-2016, 2016.

Koffi, B., Schulz, M., Bréon, F.-M., Dentener, F., Steensen, B. M., Griesfeller, J., Winker, D., Balkanski, Y., Bauer, S. E., Bellouin, N., Bernsten, T., Bian, H., Chin, M., Diehl, T., Easter, R., Ghan, S., Hauglustaine, D. A., Iversen, T., Kirkevåg, A., Liu, X., Lohmann, U., Myhre, G., Rasch, P., Seland, Ø., Skeie, R. B., Steenrod, S. D., Stier, P., Tackett, J., Takemura, T., Tsigaridis, K., Vuolo, M. R., Yoon, J., and Zhang, K.: Evaluation of the aerosol vertical distribution in global aerosol models through comparison against CALIOP measurements: AeroCom phase II results, Journal of Geophysical Research: Atmospheres, 121, 7254–7283, https://doi.org/10.1002/2015JD024639, 2016.

Kuang, Z., Margolis, J., Toon, G., Crisp, D., and Yung, Y.: Spaceborne measurements of atmospheric CO_2 by high-resolution NIR spectrometry of reflected sunlight: An introductory study, Geophysical Research Letters, 29, 11–1, https://doi.org/10.1029/2001GL014298, 2002.

Le Quéré, C., Raupach, M. R., Canadell, J. G., Marland, G., Bopp, L., Ciais, P., Conway, T. J., Doney, S. C., Feely, R. A., Foster, P., Friedlingstein, P., Gurney, K., Houghton, R. A., House, J. I., Huntingford, C., Levy, P. E., Lomas, M. R., Majkut, J., Metzl, N., Ometto, J. P., Peters, G. P., Prentice, I. C., Randerson, J. T., Running, S. W., Sarmiento, J. L., Schuster, U., Sitch, S., Takahashi, T., Viovy, N., van der Werf, G. R., and Woodward, F. I.: Trends in the sources and sinks of carbon dioxide, Nature Geoscience, 2, 831–836, https://doi.org/10.1038/ngeo689, 2009.

L'Ecuyer, T. S. and Jiang, J. H.: Touring the atmosphere aboard the A-Train, Physics Today, 63, 36–41, https://doi.org/10.1063/1.3463626, 2010.

Liu, J., Bowman, K. W., Schimel, D. S., Parazoo, N. C., Jiang, Z., Lee, M., Bloom, A. A., Wunch, D., Frankenberg, C., Sun, Y., O'Dell, C. W., Gurney, K. R., Menemenlis, D., Gierach, M., Crisp, D., and Eldering, A.: Contrasting carbon cycle responses of the tropical continents to the 2015–2016 El Niño, Science, 358, https://doi.org/10.1126/science.aam5690, 2017.

Mann, G. W., Carslaw, K. S., Reddington, C. L., Pringle, K. J., Schulz, M., Asmi, A., Spracklen, D. V., Ridley, D. A., Woodhouse, M. T., Lee, L. A., Zhang, K., Ghan, S. J., Easter, R. C., Liu, X., Stier, P., Lee, Y. H., Adams, P. J., Tost, H., Lelieveld, J., Bauer, S. E., Tsigaridis, K., van Noije, T. P. C., Strunk, A., Vignati, E., Bellouin, N., Dalvi, M., Johnson, C. E., Bergman, T., Kokkola, H., von Salzen, K., Yu, F., Luo, G., Petzold, A., Heintzenberg, J., Clarke, A., Ogren, J. A., Gras, J., Baltensperger, U., Kaminski, U., Jennings, S. G., O'Dowd, C. D., Harrison, R. M., Beddows, D. C. S., Kulmala, M., Viisanen, Y., Ulevicius, V., Mihalopoulos, N., Zdimal, V., Fiebig, M., Hansson, H.-C., Swietlicki, E., and Henzing, J. S.: Intercomparison and evaluation of global aerosol microphysical properties among AeroCom models of a range of complexity, Atmospheric Chemistry and Physics, 14, 4679–4713, https://doi.org/10.5194/acp-14-4679-2014, 2014.

Martonchik, J. V., Diner, D. J., Kahn, R. A., Ackerman, T. P., Verstraete, M. M., Pinty, B., and Gordon, H. R.: Techniques for the retrieval of aerosol properties over land and ocean using multiangle imaging, IEEE Transactions on Geoscience and Remote Sensing, 36, 1212–1227, https://doi.org/10.1109/36.701027, 1998.

Miller, C. E., Crisp, D., DeCola, P. L., Olsen, S. C., Randerson, J. T., Michalak, A. M., Alkhaled, A., Rayner, P., Jacob, D. J., Suntharalingam, P., Jones, D. B. A., Denning, A. S., Nicholls, M. E., Doney, S. C., Pawson, S., Boesch, H., Connor, B. J., Fung, I. Y., O'Brien, D., Salawitch,

R. J., Sander, S. P., Sen, B., Tans, P., Toon, G. C., Wennberg, P. O., Wofsy, S. C., Yung, Y. L., and Law, R. M.: Precision requirements for space-based X_{CO_2} data, Journal of Geophysical Research, 112, D10 314, https://doi.org/10.1029/2006JD007659, 2007.

Nelson, R. R., O'Dell, C. W., Taylor, T. E., Mandrake, L., and Smyth, M.: The potential of clear-sky carbon dioxide satellite retrievals, Atmospheric Measurement Techniques, 9, 1671–1684, https://doi.org/10.5194/amt-9-1671-2016, 2016.

5 O'Brien, D. M. and Rayner, P. J.: Global observations of the carbon budget 2. CO$_2$ column from differential absorption of reflected sunlight in the 1.61 μm band of CO$_2$, Journal of Geophysical Research, 107, ACH–6, https://doi.org/10.1029/2001JD000617, 2002.

O'Dell, C. W., Conner, B., Bösch, H., O'Brien, D., Frankenberg, C., Castano, R., Christi, M., Eldering, D., Fisher, B., Gunson, M., McDuffie, J., Miller, C. E., Natraj, V., Oyafuso, F., Polonsky, I., Smyth, M., Taylor, T., Toon, G. C., Wennberg, P. O., and Wunch, D.: The ACOS CO$_2$ retrieval algorithm - Part 1: Description and validation against synthetic observations, Atmospheric Measurement Techniques, 5, 99–121,
10 https://doi.org/10.5194/amt-5-99-2012, 2012.

O'Dell, C. W., Eldering, A., Wennberg, P. O., Crisp, D., Gunson, M. R., Fischer, B., Frankenberg, C., Kiel, M., Lindqvist, H., Mandrake, L., Merrelli, A., Natraj, V., Nelson, R. R., Osterman, G. B., Payne, V. H., Taylor, T. E., Wunch, D., Drouin, B. J., Oyafuso, F., Chang, A., McDuffie, J., Smyth, M., Baker, D. F., Basu, S., Chevallier, F., Crowell, S. M. R., Feng, L., Palmer, P. I., Dubey, M., García, O. E., Griffith, D. W. T., Hase, F., Iraci, L. T., Kivi, R., Morino, I., Notholt, J., Ohyama, H., Petri, C., Roehl, C. M., Sha, M. K., Strong, K., Sussmann,
15 R., Te, Y., Uchino, O., and Velazcu, V. A.: Improved retrievals of carbon dioxide from the orbiting carbon observatory-2 with the version 8 ACOS algorithm, Atmospheric Measurement Techniques, https://doi.org/10.5194/amt-2018-257, 2018.

Oshchepkov, S., Bril, A., and Yokota, T.: PPDF-based method to account for atmospheric light scattering in observations of carbon dioxide from space, Journal of Geophysical Research, 113, https://doi.org/10.1029/2008JD010061, 2008.

Osterman, G., Eldering, A., Mandrake, L., O'Dell, C., Wunch, D., Wennberg, P. O., Fischer, B., and
20 Marchetti, Y.: Orbiting Carbon Observatory–2 (OCO-2) Lite Files, Bias Correction, and Warn Level, Tech. rep., NASA Jet Propulsion Laboratory, California Institute of Technology, Pasadena, CA, version 2.0, https://docserver.gesdisc.eosdis.nasa.gov/public/project/OCO/OCO2_XCO2_Lite_Files_and_Bias_Correction.pdf, 2017.

Parker, R., Bösch, H., and Cogan, A.: Algorithm Theoretical Basis Document Version 2 (ATBDv2) The University of Leicester Full-Physics Retrieval Algorithm for the retrieval of X_{CO_2} and X_{CH_4}, Tech. rep., University of Leicester, Leicester, UK, version 2, 2011.

25 Peters, W., Jacobson, A. R., Sweeney, C., Andrews, A. E., Conway, T. J., Masarie, K., Miller, J. B., Bruhwiler, L. M. P., Pétron, G., Hirsch, A. I., Worthy, D. E. J., van der Werf, G. R., Randerson, J. T., Wennberg, P. O., Krol, M. C., and Tans, P. P.: An atmospheric perspective on North American carbon dioxide exchange: CarbonTracker, Proceedings of the National Academy of Science of the United States of America, 104, 18 925–18 930, https://doi.org/10.1073/pnas.0708986104, 2007.

Pougatchev, N., August, T., Calbet, X., Hultberg, T., Oduleye, O., Schlüssel, P., Stiller, B., Germain, K. S., and Bingham, G.:
30 IASI temperature and water vapor retrievals–error assessment and validation, Atmospheric Chemistry and Physics, 9, 6453–6458, https://doi.org/10.5194/acp-9-6453-2009, 2009.

Rayner, P. J. and O'Brien, D. M.: The utility of remotely sensed CO$_2$ concentration data in surface source inversions, Geophysical Research Letters, 28, 175–178, https://doi.org/10.1029/2000GL011912, 2001.

Reuter, M., Bovensmann, H., Buchwitz, M., Burrows, J. P., Heymann, J., and Schneising, O.: Algorithm Theoretical Basis Document Version
35 5 (ATBDv5) - The Bremen Optimal Estimation DOAS (BESD) algorithm for the retrieval of X_{CO_2}, Tech. rep., Institute of Environmental Physics (IUP) University of Bremen, Bremen, Germany, version 5, 2016.

Reuter, M., Buchwitz, M., Schneising, O., Noël, S., Bovensmann, H., and Burrows, J. P.: A fast atmospheric trace gas retrieval for hyperspectral instruments approximating multiple scattering—Part 2: Application to X_{CO_2} retrievals from OCO-2, Remote Sensing, 9, 1102, https://doi.org/10.3390/rs9111102, 2017.

Rienecker, M. M., Suarez, M. J., Todling, R., Bacmeister, J., Takacs, L., Liu, H.-C., Gu, W., Sienkiewicz, M., Koster, R. D., Gelaro, R.,
5   Stajner, I., and Nielsen, J. E.: The GEOS-5 Data Assimilation System-Documentation of Versions 5.0.1, 5.1.0, and 5.2.0, Tech. rep., NASA Goddard Space Flight Center, Greenbelt, MD, https://ntrs.nasa.gov/archive/nasa/casi.ntrs.nasa.gov/20120011955.pdf, 2008.

Rienecker, M. M., Suarez, M. J., Gelaro, R., Todling, R., Bacmeister, J., Liu, E., Bosilovich, M. G., Schubert, S. D., Takacs, L., Kim, G.-K., Bloom, S., Chen, J., Collins, D., Conaty, A., da Silva, A., Gu, W., Joiner, J., Koster, R. D., Lucchesi, R., Molod, A., Owens, T., Pawson, S., Pegion, P., Redder, C. R., Reichle, R., Robertson, F. R., Ruddick, A. G., Sienkiewicz, M., and Woollen, J.: MERRA: NASA's modern-
10   era retrospective analysis for research and applications, Journal of Climate, 24, 3624–3648, https://doi.org/10.1175/JCLI-D-11-00015.1, 2011.

Rödenbeck, C.: Estimating CO_2 sources and sinks from atmospheric mixing ratio measurements using a global inversion of atmospheric transport, Tech. Rep. 6, Max Planck Institue für Biogeochemie, technical Report 6, 2005.

Rodgers, C. D.: Inverse Methods for Atmospheric Sounding: Theory and Practice, World Scientific, Singapore, 2000.

15   Stocker, T. F., Qin, D., Plattner, G.-K., Tignor, M., Allen, S., Boschung, J., Nauels, A., Xia, Y., Bex, V., and Midgley, P.: IPCC, 2013: Climate Change 2013: The Physical Science Basis. Contribution of Working Group I to the Fifth Assessment Report of the Intergovernmental Panel on Climate Change, Cambridge University Press, https://doi.org/10.1017/CBO9781107415324, 2014.

Susskind, J., Barnet, C. D., and Blaisdell, J. M.: Retrieval of atmospheric and surface parameters from AIRS/AMSU/HSB data in the presence of clouds, IEEE Transactions on Geoscience and Remote Sensing, 41, 390–409, https://doi.org/10.1109/TGRS.2002.808236, 2003.

20   Sussmann, R. and Rettinger, M.: TCCON data from Garmisch (DE), Release GGG2014.R0, TCCON Data Archive, hosted by CaltechDATA, https://doi.org/10.14291/tccon.ggg2014.garmisch01.R0/1149299, 2014.

Taylor, T. E., O'Dell, C. W., Frankenberg, C., Partain, P. T., Cronk, H. Q., Savtchenko, A., Nelson, R. R., Rosenthal, E. J., Chang, A. Y., Fisher, B., Osterman, G. B., Pollock, R. H., Crisp, D., Eldering, A., and Gunson, M. R.: Orbiting Carbon Observatory-2 (OCO-2) cloud screening algorithms: Validation against collocated MODIS and CALIOP data, Atmospheric Measurement Techniques, 9, 973–989,
25   https://doi.org/10.5194/amt-9-973-2016, 2016.

Te, Y., Jeseck, P., and Janssen, C.: TCCON data from Paris (FR), Release GGG2014.R0, TCCON Data Archive, hosted by CaltechDATA, https://doi.org/10.14291/tccon.ggg2014.paris01.R0/1149279, 2014.

Warneke, T., Messerschmidt, J., Notholt, J., Weinzierl, C., Deutscher, N. M., Petri, C., Grupe, P., Vuillemin, C., Truong, F., Schmidt, M., Ramonet, M., and Parmentier, E.: TCCON data from Orléans (FR), Release GGG2014.R0, TCCON Data Archive, hosted by CaltechDATA,
30   https://doi.org/10.14291/tccon.ggg2014.orleans01.R0/1149276, 2014.

Wennberg, P. O., Roehl, C., Wunch, D., Toon, G. C., Blavier, J.-F., Washenfelder, R., Keppel-Aleks, G., Allen, N., and Ayers, J.: TCCON data from Park Falls (US), Release GGG2014.R0, TCCON Data Archive, hosted by CaltechDATA, https://doi.org/10.14291/tccon.ggg2014.parkfalls01.R0/1149161, 2014.

Wennberg, P. O., Wunch, D., Roehl, C., Blavier, J.-F., Toon, G. C., and Allen, N.: TCCON data from Caltech (US), Release GGG2014.R1,
35   TCCON Data Archive, hosted by CaltechDATA, https://doi.org/10.14291/tccon.ggg2014.pasadena01.R1/1182415, 2015.

Wennberg, P. O., Wunch, D., Roehl, C., Blavier, J.-F., Toon, G. C., and Allen, N.: TCCON data from Lamont (US), Release GGG2014.R1, TCCON Data Archive, hosted by CaltechDATA, https://doi.org/10.14291/tccon.ggg2014.lamont01.R1/1255070, 2016.

Wunch, D., Toon, G. C., Blavier, J.-F. L., Washenfelder, R. A., Notholt, J., Connor, B. J., Griffith, D. W. T., Sherlock, V., and Wennberg, P. O.: The Total Carbon Column Observing Network, Philosophical Transactions of the Royal Society A, 369, 2087–2112, https://doi.org/10.1098/rsta.2010.0240, 2011.

Yang, D., Liu, Y., Cai, Z., Chen, X., Yao, L., and Lu, D.: First Global Carbon Dioxide Maps Produced from TanSat Measurements, Advances
5   in Atmospheric Sciences, 35, 621–623, https://doi.org/10.1007/s00376-018-7312-6, 2018.

Yokota, T., Yoshida, Y., Eguchi, N., Ota, Y., Tanaka, T., Watanabe, H., and Maksyutov, S.: Global Concentrations of CO_2 and CH_4 Retrieved from GOSAT: First Preliminary Results, Scientific Online Letters on the Atmosphere, 5, 160–163, https://doi.org/10.2151/sola.2009-041, 2009.

Table 1. TCCON stations used in this study.

TCCON station	Dates Used	Reference
Ascension Island	Sep 2014–Dec 2015	Feist et al. (2014)
Caltech, Pasadena, CA, USA	Sep 2014–May 2016	Wennberg et al. (2015)
Darwin, Australia	Sep 2014–May 2016	Griffith et al. (2014)
Edwards (Armstrong), CA, USA	Sep 2014–Mar 2016	Iraci et al. (2016)
Garmisch, Germany	Sep 2014–Nov 2015	Sussmann and Rettinger (2014)
Karlsruhe, Germany	Sep 2014–May 2016	Hase et al. (2015)
Lamont, OK, USA	Sep 2014–May 2016	Wennberg et al. (2016)
Manaus, Brazil	Oct 2014–Jun 2016	Dubey et al. (2014)
Orléans, France	Sep 2014–Nov 2015	Warneke et al. (2014)
Paris, France	Sep 2014–Sep 2015	Te et al. (2014)
Park Falls, WI, USA	Sep 2014–May 2016	Wennberg et al. (2014)
Saga, Japan	Sep 2014–Feb 2016	Kawakami et al. (2014)
Sodankylä, Finland	Sep 2014–Apr 2016	Kivi and Heikkinen (2016)

Table 2. Prior uncertainties of retrieved natural log of the optical depth, σ_τ, and retrieved Gaussian heights, σ_H, for all retrieval variants. The first entry (V8 + MERRA-2 Climatological Types & AODs with high uncertainty) is equivalent to the operational ACOS retrieval uncertainties. The prior 1-sigma uncertainties on the natural log of the stratospheric AOD are slightly lower, at 1.8, 0.45, and 0.001 for the three uncertainty levels, respectively.

Retrieval Type	High Uncertainty	Low Uncertainty	No Uncertainty
V8 + MERRA-2 Climatological Types & AODs	σ_τ=2.0, σ_H=0.2	σ_τ=0.5, σ_H=0.2	σ_τ=0.001, σ_H=0.2
V8 + GEOS-5 Types & AODs	σ_τ=2.0, σ_H=0.2	σ_τ=0.5, σ_H=0.2	σ_τ=0.001, σ_H=0.2
V8 + GEOS-5 Types & Gaussian AODs/Heights	σ_τ=2.0, σ_H=0.2	σ_τ=0.5, σ_H=0.05	σ_τ=0.001, σ_H=0.0001
V8 + GEOS-5 Types & Scalar Profile	$\sigma_{\tau,\,layer}$=ln 10	$\sigma_{\tau,\,layer}$=0.5	$\sigma_{\tau,\,layer}$=0.01
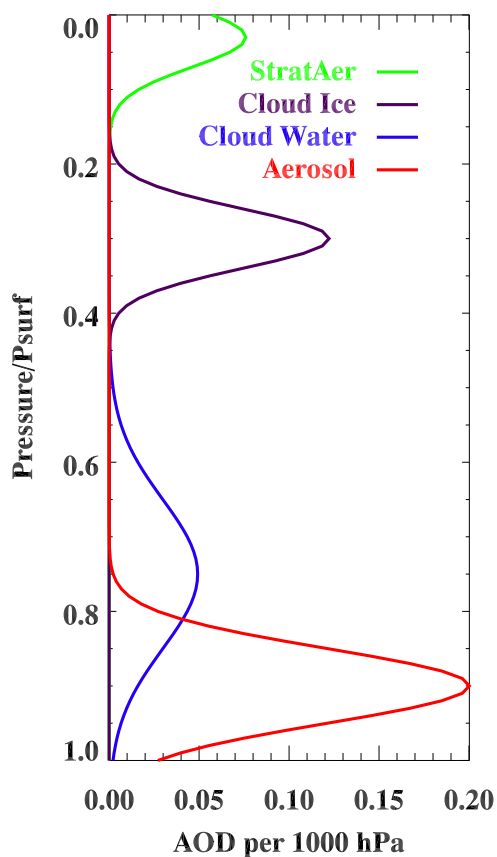
Figure 1. Prior Gaussian profiles of the lower tropospheric aerosol types (red), water cloud (blue), ice cloud (purple), and stratospheric aerosol (green). The local AOD per unit pressure at 755 nm is plotted as a function of the relative pressure. The lower tropospheric aerosol prior AOD is not fixed as for the other types, but rather is taken from a climatology described in the text. Taken from O'Dell et al., 2018.
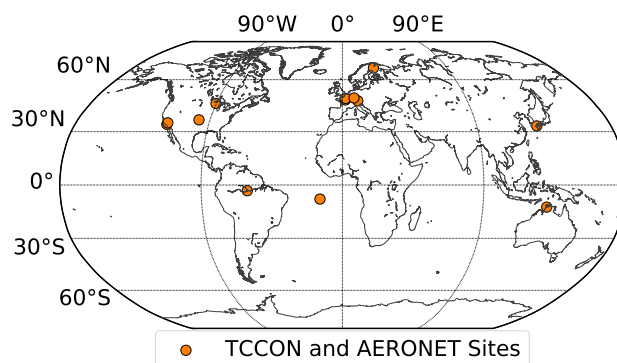
Figure 2. TCCON and AERONET sites used in this study.
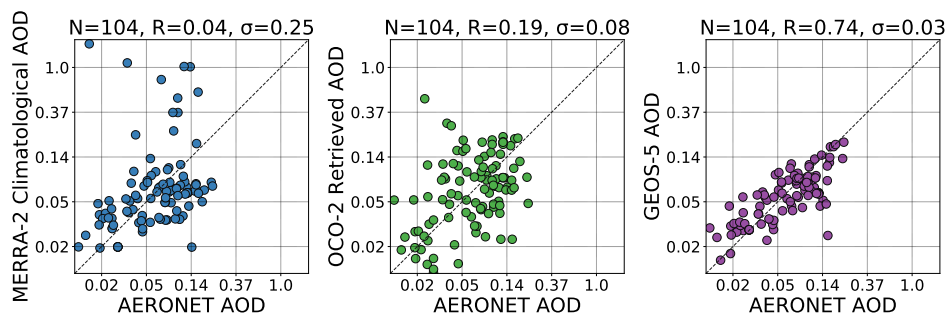
Figure 3. Left: MERRA-2 climatological AOD vs. AERONET AOD. Middle: OCO-2 V8 retrieved AOD vs. AERONET AOD. Right: GEOS-5 co-located AOD vs. AERONET AOD. The AERONET AODs are the means of the AODs at 675 nm and 870 nm. Overpass means are plotted. AERONET stations used were those present at the TCCON sites selected for this study, listed in Table 1 and shown in Fig. 2, that had valid data between 17 September 2014 and 2 May 2016.
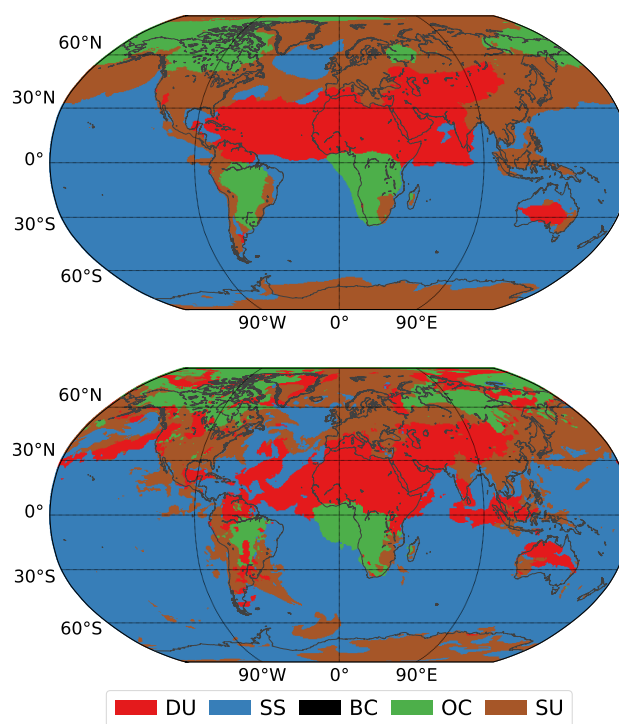
Figure 4. Top: primary aerosol type selected for the month of July using the MERRA-2 climatology. Bottom: primary GEOS-5 aerosol type selected for 1 July 2016 0Z. Aerosol types are dust (DU), sea salt (SS), black carbon (BC), organic carbon (OC), and sulfate (SU).
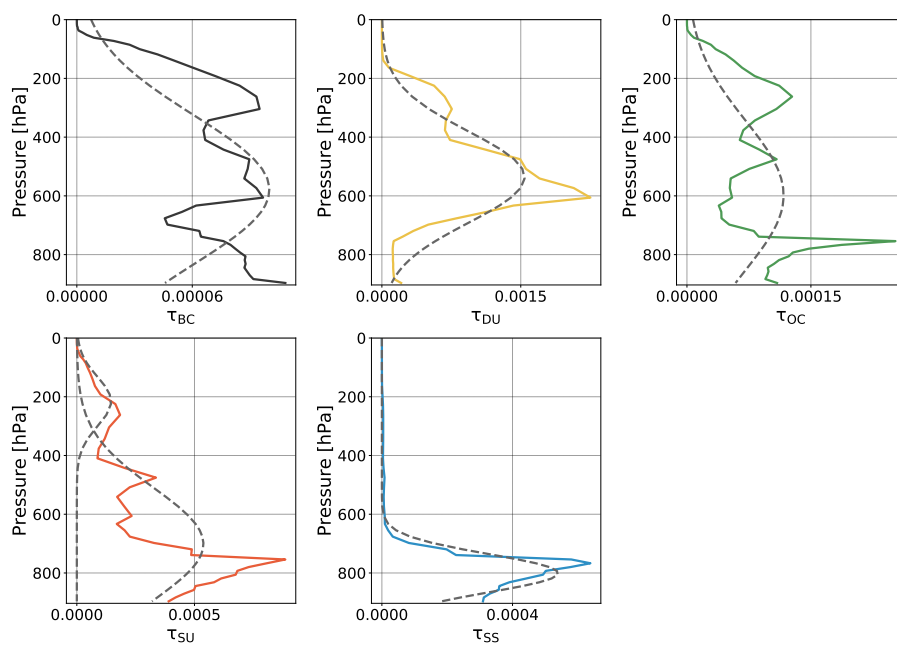
Figure 5. Example of fitting Gaussians to the GEOS-5 AOD profiles. Upper row is black carbon (black), dust (yellow), and organic carbon (green). Lower row is sulfate (orange) and sea salt (blue). Dashed grey lines are the Gaussian fits to the profiles.
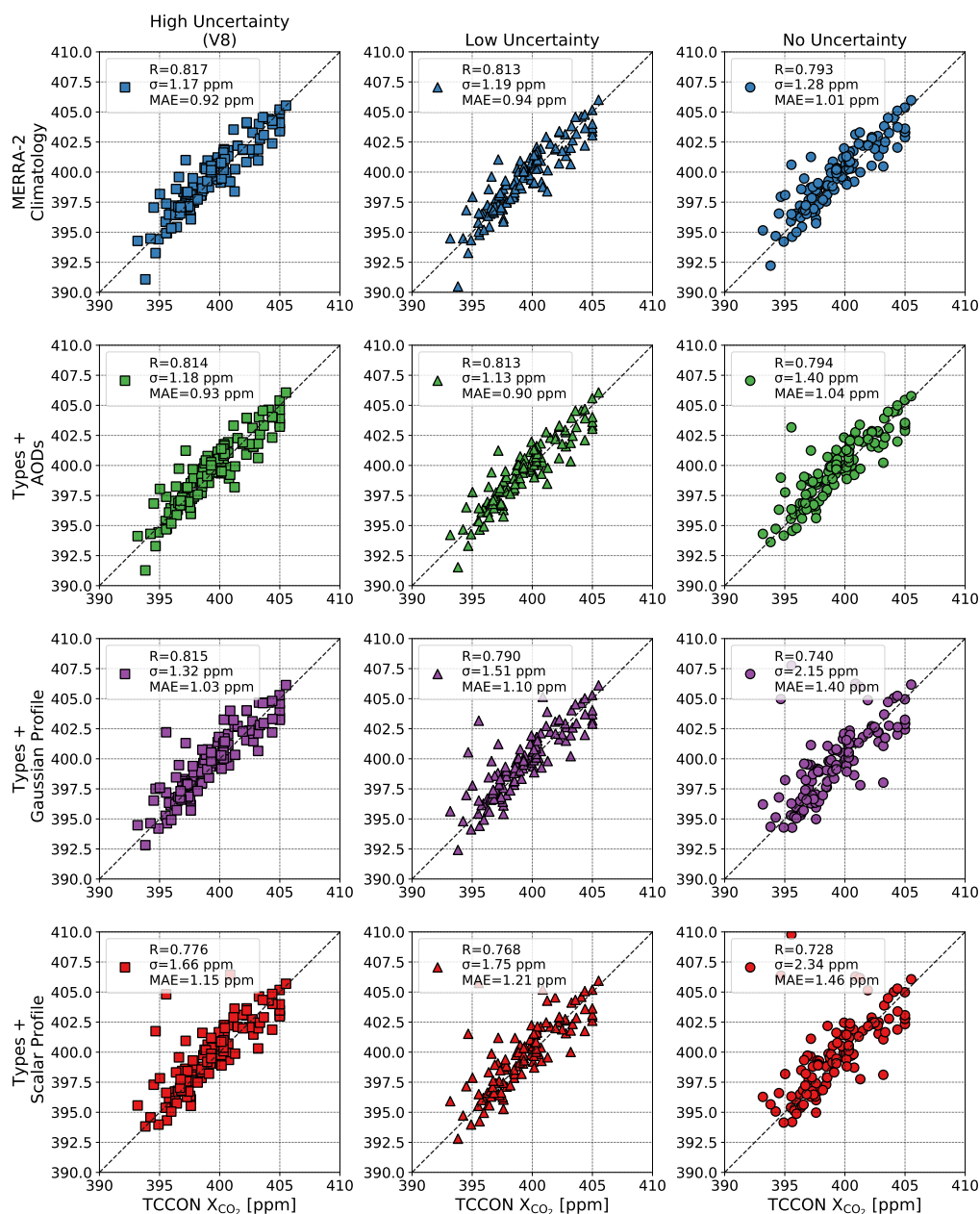
Figure 6. Retrieved OCO-2 X_{CO_2} (y-axes) against TCCON X_{CO_2} (x-axes). Overpass means are plotted. The first row is the operational retrieval (V8). The second row is ingesting GEOS-5 types and AODs, the third row is ingesting GEOS-5 types and Gaussian profile priors, and the fourth row is ingesting GEOS-5 types and solving for a scalar to the prior aerosol profile. The left column is high uncertainty, the middle column is low uncertainty, and the right column is no uncertainty (see Table 2). For each panel, R is the correlation coefficient, σ is the standard deviation of the error against TCCON, and MAE is the mean absolute error against TCCON. The TCCON sites used are listed in Table 1, shown in Fig. 2, and were required to have valid data between 17 September 2014 and 2 May 2016.
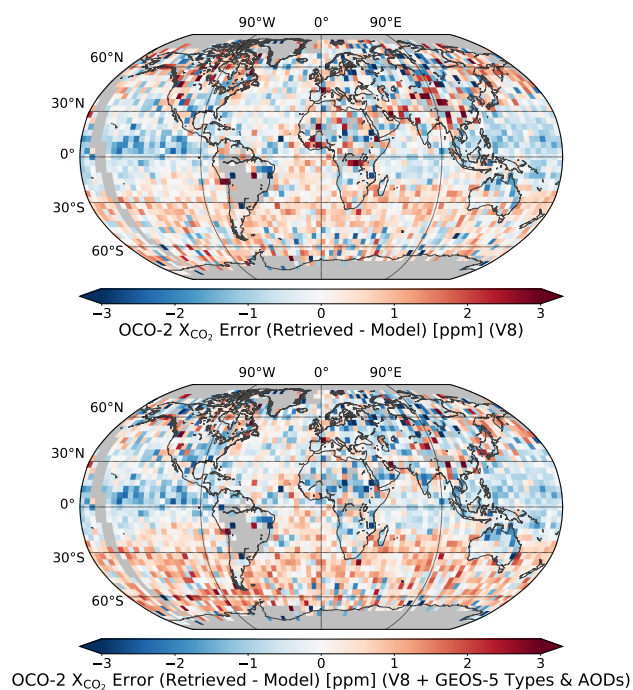
Figure 7. Top: 4x4 degree binned X_{CO_2} error against model validation for V8. Bottom: 4x4 degree binned X_{CO_2} error against model validation for the GEOS-5 types & AODs with low uncertainty setup. Grey bins represent no data.
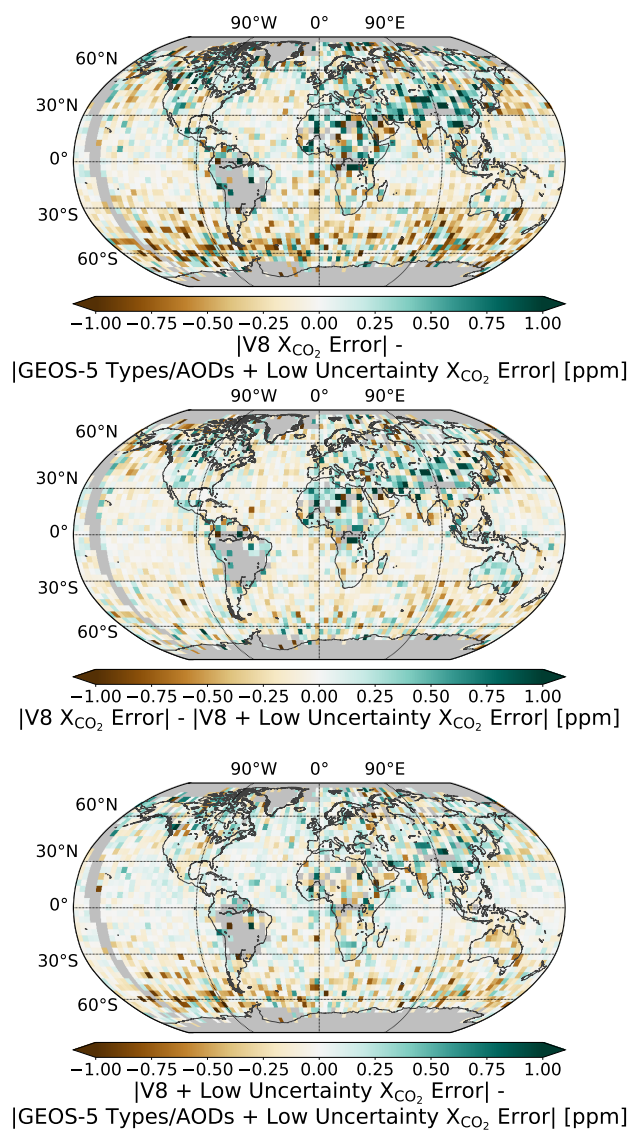
Figure 8. Top: 4x4 degree binned absolute value of V8 X_{CO_2} error against the model validation minus the absolute value of the GEOS-5 Types & AODs with low uncertainty X_{CO_2} error against the model validation. Middle: 4x4 degree binned absolute value of V8 X_{CO_2} error against the model validation minus the absolute value of V8 with low uncertainty X_{CO_2} error against the model validation. Bottom: 4x4 degree binned absolute value of V8 with low uncertainty X_{CO_2} error against the model validation minus the absolute value of GEOS-5 Types & AODs with low uncertainty X_{CO_2} error against the model validation. Green grid cells represent an improvement relative to the model validation while brown grid cells represent a worse comparison to the model validation. Grey bins represent no data.
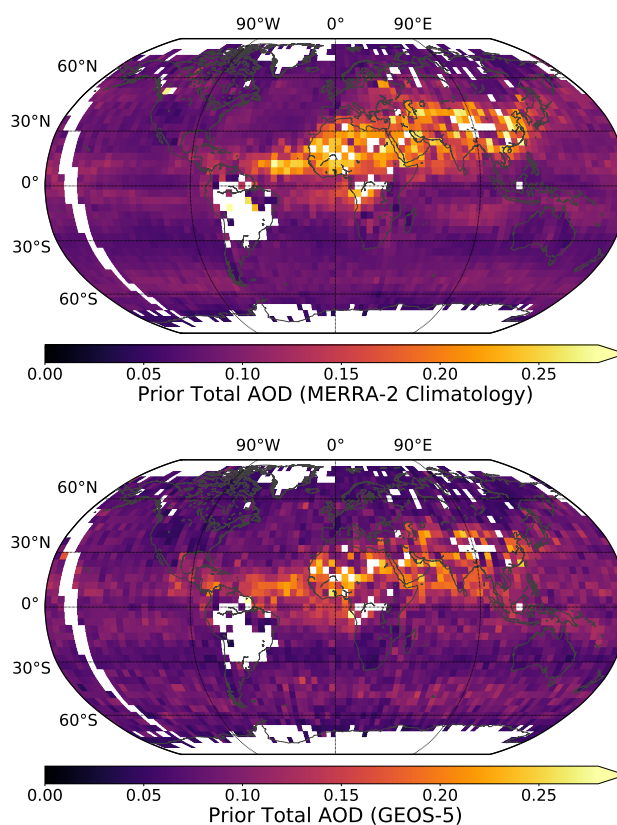
Figure 9. Top: 4x4 degree binned prior AOD for V8, derived from a MERRA-2 monthly climatology. Bottom: 4x4 degree binned prior AOD for V8 + GEOS-5 Types & AODs with low uncertainty, derived from co-located GEOS-5 AODs. White bins represent no data.
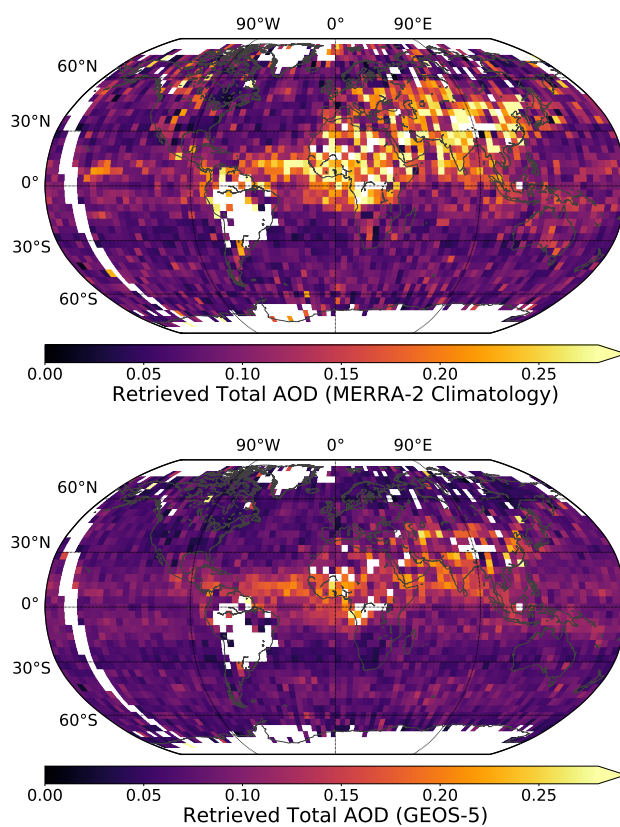
Figure 10. Top: 4x4 degree binned retrieved AOD for V8. Bottom: 4x4 degree binned retrieved AOD for V8 + GEOS-5 Types & AODs with low uncertainty. White bins represent no data.
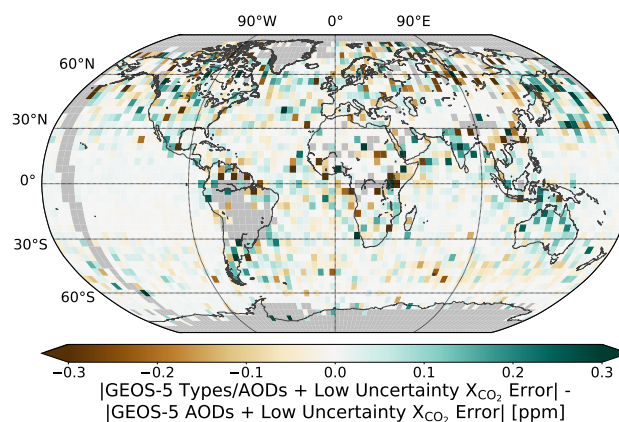
Figure 11. 4x4 degree binned absolute value of GEOS-5 Types & AODs with low uncertainty X_{CO_2} error against the model validation minus the absolute value of GEOS-5 AODs with low uncertainty X_{CO_2} error against the model validation. Green grid cells represent an improvement relative to the model validation while brown grid cells represent a worse comparison to the model validation. Grey bins represent no data.
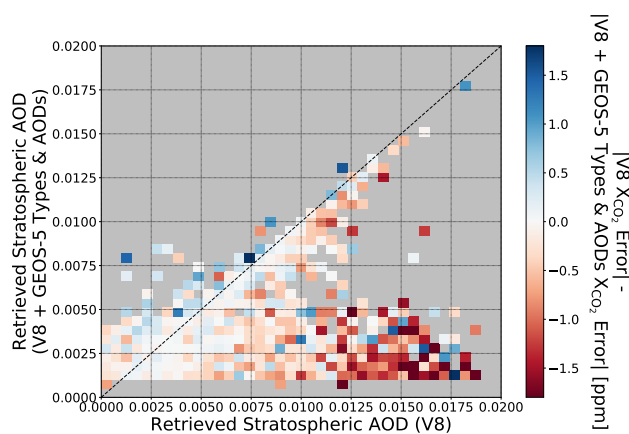
Figure 12. Retrieved stratospheric AOD from V8 versus retrieved stratospheric AOD from V8 + GEOS-5 Types & AODs with low uncertainty for the Southern Ocean. Color represents the change in the absolute value of the X_{CO_2} error between the two retrieval types, where blue demonstrates an improvement over V8 and red represents a worsening.
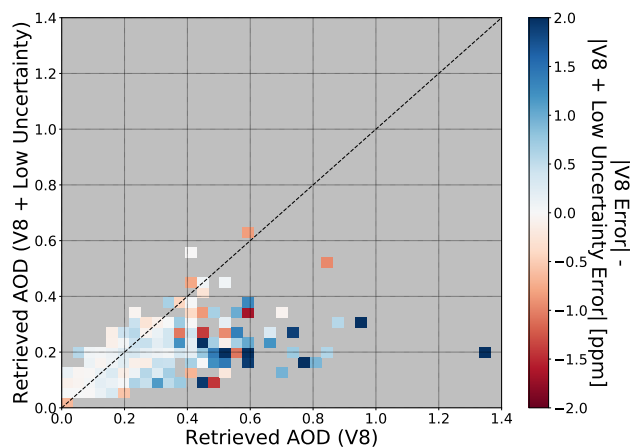
Figure 13. Retrieved AOD from V8 versus retrieved AOD from V8 with low uncertainty for North Africa and Central Asia. Color represents the change in the absolute value of the X_{CO_2} error between the two retrieval types, where blue demonstrates an improvement over V8 and red represents a worsening.